

# Novel type of atomic-scale spin lattice at a surface and its emergent Hall effect

M. Hoffmann,<sup>1,\*</sup> J. Weischenberg,<sup>2</sup> B. Dupé,<sup>1</sup> F. Freimuth,<sup>2</sup> P. Ferriani,<sup>1</sup> Y. Mokrousov,<sup>2</sup> and S. Heinze<sup>1</sup>

<sup>1</sup>*Institute of Theoretical Physics and Astrophysics, Christian-Albrechts University of Kiel, Leibnizstrasse 15, D-24098 Kiel, Germany*

<sup>2</sup>*Peter Grünberg Institut and Institute for Advanced Simulation, Forschungszentrum Jülich and JARA, Germany*  
(Dated: May 2, 2022)

We predict the occurrence of a novel type of atomic-scale spin lattice in an Fe monolayer on the Ir(001) surface. Based on density functional theory calculations we parametrize a spin Hamiltonian and solve it numerically using Monte-Carlo simulations. We find the stabilization of a three-dimensional spin structure arranged on a  $(3 \times 3)$  lattice. Despite an almost vanishing total magnetization we predict the emergence of a large anomalous Hall effect, to which there is a significant topological contribution purely due to the real space spin texture at the surface.

Localized stable spin textures such as skyrmions or chiral domain walls have attracted much attention recently due to their unique topological and transport properties [1–3] and potential applications in spintronics [4–7]. A key ingredient for their occurrence is the Dzyaloshinskii-Moriya (DM) interaction [8, 9], which arises due to spin-orbit interaction in systems with broken inversion symmetry, as in the bulk of non-centrosymmetric crystals or at surfaces and interfaces. Hall effects play an important role in these systems. For instance, the spin-orbit torque originating from the spin Hall effect drives the motion of chiral domain walls in ultrathin films very efficiently and very high speeds have been reported [2, 3]. The topological Hall effect, defined as the contribution to the Hall resistivity due to chiral spin texture, serves as one of the main tools to pinpoint the skyrmion phase in the phase diagram of bulk alloys such as MnSi or FeGe [10–12].

The topological Hall effect in complex large-scale magnetic structures is normally described assuming the adiabatic viewpoint of infinitesimally slowly varying spin texture [1]. For skyrmions, the topological Hall resistivity can be factorized into the product of an emergent magnetic field, which is the direct consequence of the non-zero topological charge, and the topological Hall coefficient  $R^{\text{top}}$ , which can be determined from the electronic structure of the ferromagnetic crystal [10, 13]. The validity of this picture has been demonstrated for large-scale skyrmions in bulk  $\text{Mn}_x\text{Fe}_{1-x}\text{Si}$  alloys [14]. On the other side of the length scale, the chirality-driven contribution to the anomalous Hall effect (AHE) has been predicted and observed in bulk strongly-frustrated correlated oxides and bulk antiferromagnets, which exhibit non-collinear magnetic order on the scale of 1 nm [15–22].

Chiral domain walls and skyrmions with an extent of down to 1 nm can also occur at transition-metal interfaces and surfaces [23–26]. It has been demonstrated that higher-order exchange interactions can play a crucial role in such systems. They enforce the atomic-scale skyrmion lattice observed for an Fe monolayer on the Ir(111) surface [25] and a conical spin spiral phase for a Mn double layer on W(110) [27]. However, to date, very little is

known both experimentally and theoretically about the Hall effects in such complex nanometer-scale spin textures at surfaces and interfaces.

Here, we present a model system for a novel type of atomic-scale spin lattice at a transition-metal surface and study its transport properties. In contrast to systems explored so far for skyrmion spin textures the local exchange interaction is antiferromagnetic in this system. Based on density-functional theory (DFT) and Monte-Carlo simulations, we find a complex three-dimensional spin structure on a  $(3 \times 3)$  lattice for an Fe monolayer on Ir(001), which has been shown to grow pseudomorphically [28]. This spin texture with angles close to  $120^\circ$  between adjacent spins arises due to the coupling of spin spirals stabilized by exchange and DM interaction via the four-spin interaction. Using DFT we demonstrate that, despite very small total magnetization, this non-trivial  $(3 \times 3)$  spin lattice gives rise to the AHE, essentially larger than that observed in non-collinear bulk compounds [15–22]. We further show the existence in this system of a sizeable surface “topological” contribution to the AHE and orbital magnetization, which originate purely in the non-trivial real-space spin distribution and do not rely on the presence of spin-orbit interaction.

Nanoscale spin textures at transition-metal interfaces [25, 29–31] can be treated employing a Hamiltonian on the discrete atomic lattice

$$\begin{aligned}
 H = & - \sum_{ij} J_{ij} (\mathbf{M}_i \cdot \mathbf{M}_j) - \sum_{ij} \mathbf{D}_{ij} \cdot (\mathbf{M}_i \times \mathbf{M}_j) \\
 & - \sum_{ijkl} K_{ijkl} [(\mathbf{M}_i \cdot \mathbf{M}_j)(\mathbf{M}_k \cdot \mathbf{M}_l) + \dots] \\
 & - \sum_{ij} B_{ij} (\mathbf{M}_i \cdot \mathbf{M}_j)^2 + \sum_i K_{\perp} (M_i^z)^2
 \end{aligned} \tag{1}$$

which describes the magnetic interactions between the magnetic moments  $\mathbf{M}_i$  of atoms at sites  $\mathbf{R}_i$ . For the Fe monolayer on Ir(001), we used DFT to obtain the parameters for the exchange interaction ( $J_{ij}$ ), the DM interaction ( $\mathbf{D}_{ij}$ ), the four-spin interaction ( $K_{ijkl}$ ) and the biquadratic exchange ( $B_{ij}$ ) as well as a uniaxial magnetocrystalline anisotropy ( $K_{\perp}$ ). We applied the projector

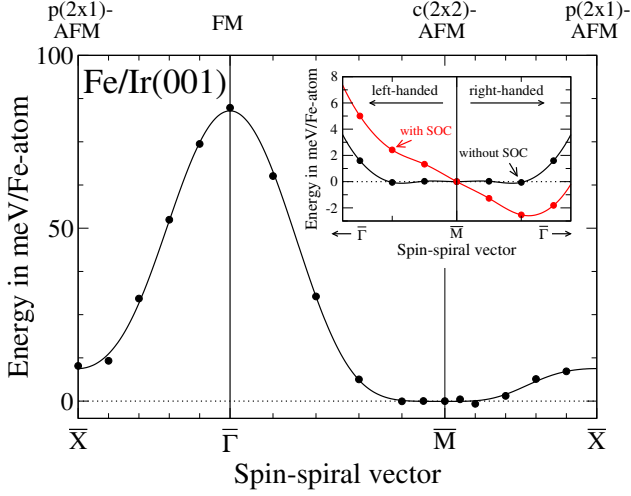


FIG. 1: Energy dispersion of homogeneous flat spin spirals for Fe/Ir(001). The energies  $E(\mathbf{q})$  (filled circles) are calculated via DFT along the high symmetry lines of the two-dimensional Brillouin zone and given with respect to the  $c(2 \times 2)$  antiferromagnetic state. The solid lines are fits to the Heisenberg model with up to sixth nearest-neighbors [36]. The inset shows the energy dispersion close to the  $\bar{M}$  point for left- and right-rotating spirals including SOC, i.e. the effect of the DM interaction.

augmented wave (PAW) method [32] as implemented in the VASP code [33, 34]. Computational details are given in the supplementary material.

To determine the exchange constants  $J_{ij}$ , we have considered flat spin spirals in which the magnetic moments are confined in a plane with a constant angle between moments at adjacent lattice sites propagating along high symmetry directions of the surface. Such a spin spiral can be characterized by a wave vector  $\mathbf{q}$  from the two-dimensional Brillouin zone (BZ) and the magnetic moment of an atom at site  $\mathbf{R}_i$ , given by  $\mathbf{M}_i = M(\sin(\mathbf{q}\mathbf{R}_i), \cos(\mathbf{q}\mathbf{R}_i), 0)$  with the size of the magnetic moment  $M$ .

The calculated energy dispersion  $E(\mathbf{q})$  of spin spirals for Fe/Ir(001) is displayed in Fig. 1. At the high symmetry points we obtain collinear spin structures: the ferromagnetic state at  $\bar{\Gamma}$ , the  $c(2 \times 2)$  antiferromagnetic state at  $\bar{M}$ , and the  $p(2 \times 1)$  antiferromagnetic state at  $\bar{X}$ . Clearly, the  $c(2 \times 2)$  antiferromagnetic state is lowest in energy among the considered collinear states in agreement with previous DFT studies [35]. The energy dispersion is very flat in the vicinity of the  $\bar{M}$ -point due to the frustration of exchange interactions. A fit to the Heisenberg model, i.e. the first term in Eq. (1), with  $J_{ij}$ 's up to sixth nearest neighbors [36] leads to an excellent description as shown by the solid line in Fig. 1 [37].

Note, that the energy dispersion of Fe/Ir(001) is almost inverted with respect to Fe/Ir(111) where the energy dispersion is flat around the  $\bar{\Gamma}$ -point, i.e. the ferromagnetic state [25, 38]. Therefore, we can also expect complex

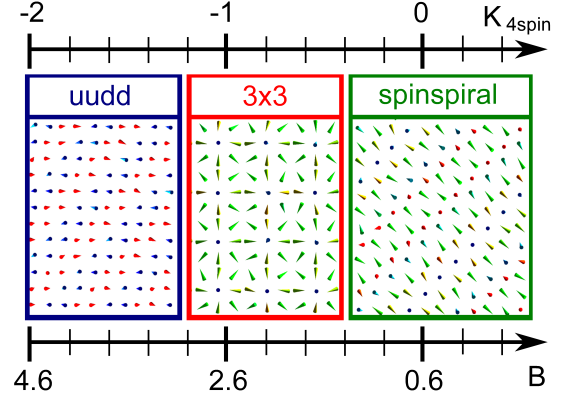


FIG. 2: Spin structures of lowest energy obtained via Monte-Carlo simulations as a function of the strength of the four-spin interaction. The biquadratic interaction is changed according to the condition  $2K_{4\text{spin}} + B = 0.7$  meV from the DFT calculations. The sketches only display a small section of the actually simulated spin lattice.

three-dimensional spin structures to occur here but of different type due to the nearest-neighbor antiferromagnetic exchange.

By taking spin-orbit coupling (SOC) into account, we can determine the magnetocrystalline anisotropy energy (MAE) defined as the energy difference between configurations with different orientation of the magnetization. For the collinear state of lowest energy, i.e. the  $c(2 \times 2)$  antiferromagnetic state, we found an easy out-of-plane axis with a MAE of  $K_{\perp} = -0.25$  meV.

At a surface SOC also induces the DM interaction [39, 40]. In order to determine its strength, we have calculated the total energy of a  $120^\circ$  spin spiral along the  $\bar{\Gamma}\bar{M}$ -direction in a  $(3 \times 1)$  super cell including SOC both with a left-handed and a right-handed rotational sense. We find that spin spirals with a right-handed rotational sense are lower by 7.3 meV/Fe atom. This energy difference allows to calculate the value of the DM interaction within the nearest-neighbor approximation which results in a value of  $D_1 = 1.5$  meV. Including the DM interaction into the energy dispersion of spin spirals leads to an energy minimum at an angle of about  $138^\circ$  between adjacent spins as shown in the inset of Fig. 1.

From the energy dispersion of spin spirals, only the Heisenberg-type exchange can be obtained. The impact of higher-order spin interactions can be determined by considering superposition states of two spin spirals. If only Heisenberg-type exchange played a role all of these spin states would be degenerate in energy. However, our DFT calculations show considerable energy differences on the order of a few meV/Fe-atom (see supplementary material). From these calculations, we determine that the nearest-neighbor four-spin,  $K_{4\text{spin}}$ , and biquadratic,  $B$ , interaction fulfill the condition  $2K_{4\text{spin}} + B = 0.7$  meV.

The energy functional Eq. (1) with the parameters

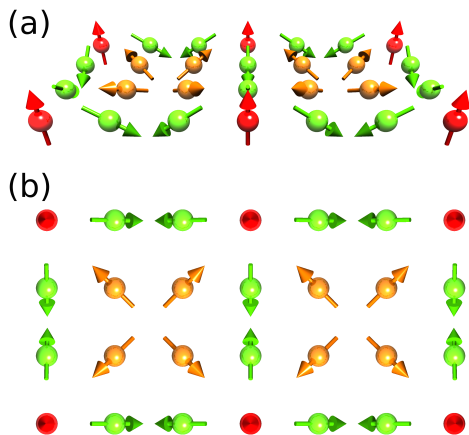


FIG. 3: (a) Side view and (b) top view of the proposed atomic-scale  $(3 \times 3)$  spin lattice. Two unit cells are shown.

from DFT can be minimized using Monte-Carlo simulations based on the Metropolis algorithm. We have chosen a spin lattice of  $(66 \times 66)$  spins and used periodic boundary conditions. We have checked the impact of the lattice size and of using open boundary conditions and found no effect on the obtained ground state. In order to explore the impact of the higher-order spin interactions, which are not univocally determined by our DFT calculations as discussed above, we have chosen different values of  $B$  and  $K_{4\text{spin}}$  that are in accordance with the condition given above. We changed the value of the four-spin interaction in steps of 0.1 meV and the biquadratic interaction and  $J_3$  were modified accordingly [36].

We found three different types of ground states depending on the value of  $K_{4\text{spin}}$  as shown in Fig. 2. A large biquadratic interaction results in a so-called up-up-down-down (*uudd*) state since a collinear alignment of neighboring spins is preferred. However, if the biquadratic interaction is reduced we find an atomic-scale non-collinear  $(3 \times 3)$  spin lattice that is stabilized by the four-spin term. For a value of  $K_{4\text{spin}} > -0.4$  meV the four-spin term cannot couple the spin spirals and we obtain a spin spiral ground state with an angle of about  $140^\circ$  between adjacent spins.

As shown in Fig. 2, the novel  $(3 \times 3)$  spin lattice can occur for a large range of values of the four-spin interaction. Its spin structure is shown in Fig. 3. The spins at the corners of the unit cell point upwards perpendicular to the surface while the spins along the sides rotate with an angle of  $\approx 123^\circ$  from the surface normal. The four spins in the center of the cell point towards the corners and with an angle of  $\approx 22^\circ$  out of the film plane.

The occurrence of this three-dimensional spin structure can be understood from the interplay of the different interactions. The combination of exchange and DM interaction leads to a spin spiral with an angle of approximately  $120^\circ$  between adjacent spins and thus a periodic-

ity of 3 atoms (cf. Fig. 1). For Fe biatomic chains on the  $(5 \times 1)$  reconstructed Ir(001) surface, such a spin spiral state has been experimentally observed [24]. In the Fe monolayer on Ir(001), the four-spin interaction can couple these spin spirals into a square lattice. Note, that there is an opposite rotational sense of the spin rotation along the side and the diagonal of the unit cell. This results from the antiferromagnetic exchange coupling between nearest neighbors which is stronger than the DM interaction that would prefer a unique rotational sense along both directions. Due to this peculiar competition of DMI and Heisenberg exchange, the spin lattice is extremely stable in an external magnetic field and cannot be destroyed up to 80 T as found in our MC simulations. The transition temperature to the paramagnetic state is obtained at approximately 60 K.

To investigate whether the  $(3 \times 3)$  spin texture results in non-trivial transport properties, we compute from first principles [41] the intrinsic Berry curvature contribution to the  $xy$ -component of the anomalous Hall conductivity (AHC) in the system  $\sigma_{3 \times 3}^{\text{AH}} = \frac{e^2 \hbar}{(2\pi)^2} \int_{BZ} \Omega_{xy}(\mathbf{k}) d\mathbf{k}$  [42], where

$$\Omega_{xy}(\mathbf{k}) = \sum_{n < E_F} \sum_{m \neq n} 2\text{Im} \frac{\langle \psi_{n\mathbf{k}} | v_x | \psi_{m\mathbf{k}} \rangle \langle \psi_{m\mathbf{k}} | v_y | \psi_{n\mathbf{k}} \rangle}{(\varepsilon_{m\mathbf{k}} - \varepsilon_{n\mathbf{k}})^2} \quad (2)$$

is the Berry curvature of occupied states with  $\psi_{n\mathbf{k}}$  as the Bloch states with corresponding energies  $\varepsilon_{n\mathbf{k}}$ , and  $v_i$  is the  $i$ 'th Cartesian component of the velocity operator. The results of our calculations for  $\sigma_{3 \times 3}^{\text{AH}}$ , presented in Fig. 4 as a function of the substrate thickness, indicate a sizeable AHE in the  $(3 \times 3)$  spin lattice state with the magnitude similar to that of bulk transition-metal ferromagnets [42–44]. The large variation of the AHC with thickness, apparent from Fig. 4, is typical for such effects as the AHE, spin Hall effect or the spin-orbit torque in the limit of ultrathin films [43, 45, 46].

In the context of thin magnetic layers of transition-metals on paramagnetic substrates, the emergence of the large  $\sigma_{3 \times 3}^{\text{AH}}$  appears rather surprising, since the total magnetization of the system in the  $(3 \times 3)$  state is almost vanishing. By artificially rotating the spin moments on the Fe atoms slightly away from their equilibrium directions we acquire a complete suppression of the magnetization and observe that the values of  $\sigma_{3 \times 3}^{\text{AH}}$  stay very close to those with small uncompensated magnetization. This clearly distinguishes our case from the case of the AHE in collinear magnets, which relies on non-vanishing macroscopic magnetization and presence of SOC [42].

Another remarkable observation is that a large contribution to  $\sigma_{3 \times 3}^{\text{AH}}$  is provided even without taking the SOC into account, as apparent from Fig. 4, where the values of the intrinsic AHC, computed with the SOC explicitly switched off in our calculations, are presented in comparison with  $\sigma_{3 \times 3}^{\text{AH}}$ . Since the AHE vanishes for any collinear magnetic state of our system without SOC,

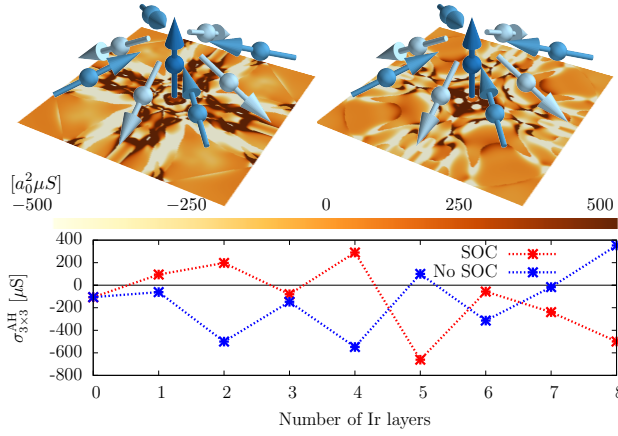


FIG. 4: Top: BZ distribution of the Berry curvature without (left) and with (right) SOC for Fe monolayer in  $(3 \times 3)$  state with one layer of Ir substrate, superimposed with the real-space distribution of the spins (blue arrows). Bottom: calculated values of  $\sigma_{3 \times 3}^{AH}$  as function of the Ir substrate thickness.

it allows us to define the contribution to  $\sigma_{3 \times 3}^{AH}$  without SOC as the “topological” contribution to the AHC,  $\sigma_{3 \times 3}^{TH}$ , which stems purely from the spin texture in real space, and which does not rely on the presence of SOC. The particular symmetry of our system which results in non-vanishing  $\sigma_{3 \times 3}^{TH}$ , also gives rise to a finite local scalar spin chirality  $\mathbf{M}_i \cdot (\mathbf{M}_j \times \mathbf{M}_k)$ , non-vanishing when integrated over the unit cell [20]. To distinguish our case from the case of large two-dimensional skyrmions and bulk frustrated oxides, for which topological contribution to the Hall effect in some cases can be described neglecting the spin-orbit effects [13, 14, 19–21], for our class of systems we call the corresponding anomalous Hall effect without SOC the *surface topological Hall effect*. Our calculations suggest the existence of surface THE in transition-metal multilayers.

Ultimately, the large values of  $\sigma_{3 \times 3}^{TH}$  are due to a direct effect of the non-trivial real-space distribution of spin on reciprocal-space distribution of the AHC, given by the Berry curvature [47]. To convince ourselves in this explicitly, we plot in Fig. 4 the Brillouin zone distribution of the Berry curvature computed with and without SOC for the system of an Fe layer in the  $(3 \times 3)$  spin state on one layer of the Ir substrate. As apparent from the case without SOC, there is a very close correlation of the Berry curvature distribution with the spin-distribution in real-space, while the effect of SOC is to provide an additional fine structure to this distribution stemming from SOC-induced band splittings in the vicinity of the Fermi level. Thus the surface THE is more complex than the THE in large-scale skyrmions for which the topological contribution to the THE – the emergent field – can be separated from the electronic effects in a collinear host encoded in  $R^{\text{top}}$  [10, 14]. The surface THE arises from a close inter-

twining of the real and reciprocal space topology, which together play a role of a single multi-dimensional topological object with non-trivial transport properties.

The microscopic origin of the competition between non-collinearity and spin-orbit interaction for the AHE in such non-trivial surface spin textures as considered here, presents an exciting direction to study both theoretically and experimentally [48, 49]. In particular, we conjecture that the surface THE is commonly an important part of the AHE exhibited by complex spin structures at surfaces, such as nanoskyrmions [25]. One of its prominent manifestations would be the contribution to the orbital magnetization at the surface which is not originated in spin-orbit coupling [22, 50]. The orbital magnetization and the Hall effect have the same symmetry and indeed, our calculations reveal the formation of non-vanishing local atomic orbital moments at the surface of our system without spin-orbit. Without SOC, the magnitude of the maximal local orbital moment among the Fe atoms ranges from  $-0.13 \mu_B$  to  $0.03 \mu_B$  depending on the substrate thickness, which is similar in magnitude to that obtained with spin-orbit interaction included. Such “topological” orbital magnetization could be readily addressed experimentally by surface techniques.

B.D. and S.H. thank the Deutsche Forschungsgemeinschaft for financial support under project DU1489/2-1. Y.M., F.F. and J.W. acknowledge funding under HGF Programme VH-NG 513 and DFG SPP 1568. We gratefully acknowledge Jülich Supercomputing Centre, RWTH Aachen University and HLRN for providing computational resources. It is our pleasure to thank Gustav Bihlmayer for many insightful discussions.

\* Electronic address: hoffmann@theo-physik.uni-kiel.de

- [1] N. Nagaosa and Y. Tokura, *Nature Nanotech.* **8**, 899 (2013).
- [2] K.-S. Ryu, L. Thomas, S.-H. Yang, and S. Parkin, *Nature Nanotech.* **8**, 527 (2013).
- [3] S. Emori, U. Bauer, S.-M. Ahn, E. Martinez, and G. S. D. Beach, *Nature Mat.* **12**, 611 (2013).
- [4] M. Hayashi, L. Thomas, R. Moriya, C. Rettner, and S. S. P. Parkin, *Science* **320**, 209 (2008).
- [5] N. Kiselev, A. N. Bogdanov, R. Schäfer, and U. K. Rößler, *J. Phys. D* **44**, 392001 (2011).
- [6] A. Fert, V. Cros, and J. Sampaio, *Nature Nanotech.* **8**, 152 (2013).
- [7] J. Sampaio, V. Cros, S. Rohart, A. Thiaville, and A. Fert, *Nature Nanotech.* **8**, 839 (2013).
- [8] I. E. Dzyaloshinskii, *Sov. Phys. JETP* **5**, 1259 (1957).
- [9] T. Moriya, *Phys. Rev.* **120**, 91 (1960).
- [10] A. Neubauer, C. Pfleiderer, B. Binz, A. Rosch, R. Ritz, P. G. Niklowitz, and P. Böni, *Phys. Rev. Lett.* **102**, 186602 (2009).
- [11] S. Huang and C. Chien, *Phys. Rev. Lett.* **108**, 267201 (2012).
- [12] N. Kanazawa, Y. Onose, T. Arima, D. Okuyama,

- K. Ohoyama, S. Wakimoto, K. Kakurai, S. Ishiwata, and Y. Tokura, *Phys. Rev. Lett.* **106**, 156603 (2011).
- [13] P. Bruno, V. Dugaev, and M. Taillefumier, *Phys. Rev. Lett.* **93**, 096806 (2004).
- [14] C. Franz, F. Freimuth, A. Bauer, R. Ritz, C. Schnarr, C. Duvinage, T. Adams, S. Blügel, A. Rosch, Y. Mokrousov, et al., *Phys. Rev. Lett.* **112**, 186601 (2014).
- [15] C. Sürgers, G. Fischer, P. Winkel, and H. Löhneysen, *Nature Comm.* **5**, 3400 (2014).
- [16] H. Chen, Q. Niu, and A. MacDonald, *Phys. Rev. Lett.* **112**, 017205 (2014).
- [17] T. Tomizawa and H. Kontani, *Phys. Rev. B* **80**, 100401 (2009).
- [18] T. Tomizawa and H. Kontani, *Phys. Rev. B* **82**, 104412 (2010).
- [19] Y. Machida, S. Nakatsuji, Y. Maeno, T. Tayama, T. Sakakibara, and S. Onoda, *Phys. Rev. Lett.* **98**, 057203 (2007).
- [20] Y. Taguchi, Y. Oohara, H. Yoshizawa, N. Nagaosa, and Y. Tokura, *Science* **291**, 2573 (2001).
- [21] Y. Machida, S. Nakatsuji, S. Onoda, T. Tayama, and T. Sakakibara, *Nature* **463**, 210 (2010).
- [22] R. Shindou and N. Nagaosa, *Phys. Rev. Lett.* **87**, 116801 (2001).
- [23] M. Heide, G. Bihlmayer, and S. Blügel, *Physica B* **404**, 2678 (2009).
- [24] M. Menzel, Y. Mokrousov, R. Wieser, J. E. Bickel, E. Vedmedenko, S. Blügel, S. Heinze, K. von Bergmann, A. Kubetzka, and R. Wiesendanger, *Phys. Rev. Lett.* **108**, 197204 (2012).
- [25] S. Heinze, K. von Bergmann, M. Menzel, J. Brede, A. Kubetzka, R. Wiesendanger, G. Bihlmayer, and S. Blügel, *Nature Physics* **7**, 713 (2011).
- [26] N. Romming, C. Hanneken, M. Menzel, J. E. Bickel, B. Wolter, K. von Bergmann, A. Kubetzka, and R. Wiesendanger, *Science* **341**, 636 (2013).
- [27] Y. Yoshida, S. Schröder, P. Ferriani, D. Serrate, A. Kubetzka, K. von Bergmann, S. Heinze, and R. Wiesendanger, *Phys. Rev. Lett.* **108**, 087205 (2012).
- [28] V. Martin, W. Meyer, C. Giovanardi, L. Hammer, K. Heinz, Z. Tian, D. Sander, and J. Kirschner, *Phys. Rev. B* **76**, 205418 (2007).
- [29] B. Dupé, M. Hoffmann, C. Paillard, and S. Heinze, *Nature Comm.* **5**, 4030 (2014).
- [30] E. Simon, K. Palotás, L. Rózsa, L. Udvardi, and L. Szunyogh, *Phys. Rev. B* **90**, 094410 (2014).
- [31] S. Polesya, S. Mankovsky, S. Bornemann, D. Ködderitzsch, J. Minár, and H. Ebert, *Phys. Rev. B* **89**, 184414 (2014).
- [32] P. E. Blöchl, *Phys. Rev. B* **50**, 17953 (1994).
- [33] G. Kresse and J. Furthmüller, *Phys. Rev. B* **54**, 11169 (1996).
- [34] G. Kresse and D. Joubert, *Phys. Rev. B* **59**, 1758 (1999).
- [35] F. Máca, J. Kudrnovský, V. Drchal, and J. Redinger, *Phys. Rev. B* **88**, 045423 (2013).
- [36] We have obtained the following values of the exchange constants  $J_n$  between  $n$ -th nearest neighbors in the Fe monolayer on Ir(001):  $J_1 \dots J_6 = -9.44, -4.06, -1.59, -0.51, 0.01, 0.18$  meV. Note, that we can only determine the value  $J_3 + 0.5B = -1.59$  meV from the fitting where  $B$  is the nearest-neighbor bi-quadratic exchange interaction.
- [37] We have checked the influence of the Ir film thickness on the energy dispersion of spin spirals up to 15 Ir layers and found convergence of the exchange parameters for 11 Ir layers.
- [38] K. von Bergmann, S. Heinze, M. Bode, E. Y. Vedmedenko, G. Bihlmayer, S. Blügel, and R. Wiesendanger, *Phys. Rev. Lett.* **96**, 167203 (2006).
- [39] A. Crépieux and C. Lacroix, *J. Magn. Magn. Mater.* **182**, 341 (1998).
- [40] M. Bode, M. Heide, K. von Bergmann, P. Ferriani, S. Heinze, G. Bihlmayer, A. Kubetzka, O. Pietzsch, S. Blügel, and R. Wiesendanger, *Nature* **447**, 190 (2007).
- [41] See supplementary information.
- [42] N. Nagaosa, J. Sinova, S. Onoda, A. MacDonald, and N. Ong, *Rev. Mod. Phys.* **82**, 1539 (2010).
- [43] P. Czaja, F. Freimuth, J. Weischenberg, S. Blügel, and Y. Mokrousov, *Phys. Rev. B* **89**, 014411 (2014).
- [44] The values of the AHC in units of S/cm can be obtained by dividing the values in Fig. 4 with the thickness of the film, and they lie in the range between several hundreds and several thousands S/cm, depending on the thickness. For example, in case of 3-layer thick Ir substrate (0.82 nm total thickness) the total AHC constitutes  $-98$  S/cm.
- [45] F. Freimuth, S. Blügel, and Y. Mokrousov, *Phys. Rev. B* **90**, 174423 (2014).
- [46] N. H. Long, P. Mavropoulos, B. Zimmermann, D. S. G. Bauer, S. Blügel, and Y. Mokrousov, *Phys. Rev. B* **90**, 064406 (2014).
- [47] Z. Fang, N. Nagaosa, K. S. Takahashi, A. Asamitsu, R. Mathieu, T. Ogasawara, H. Yamada, M. Kawasaki, Y. Tokura, and K. Terakura, *Science* **302**, 92 (2003).
- [48] R. Cheng and Q. Niu, *Phys. Rev. B* **86**, 245118 (2012).
- [49] O. Gomonay, arXiv:1501.01189.
- [50] J. Shi, G. Vignale, D. Xiao, and Q. Niu, *Phys. Rev. Lett.* **99**, 197202 (2007).